Numerical Analysis and Performance improvement of Nanostructured Cu_2O/TiO_2 pn heterojunction Solar Cells using SCAPS

Kingsley Ukoba1[1], Patrick Ehi Imoisili[1] and Tien-Chien Jen[1]

[1]*Mechanical Engineering Science Department, University of Johannesburg, Auckland Park, South Africa*

Abstract

This paper reported numerical analysis and performance improvement of nanostructured Cu_2O/TiO_2 pn heterojunction solar cells. Metal oxides thin films including Copper oxides are promising materials for photovoltaic applications. Although, the efficiency is still lower than other solar cells materials. This paper focused on improving the efficiency of Cu_2O/TiO_2 solar cells using SCAPS simulation tool. This was done by varying the effect of film surface thickness and effect of varying deposition temperature on the solar cells. The aim of the study is to serve as a theoretical guide for laboratory research on the improvement of efficiency of Cu_2O metal oxide solar cells. The solar cells equations were modelled and thereafter theoretical validation of the nanostructured metal oxides was performed. The model working points input power of 100 mW/m^2 using an illumination of AM1.5 lamp. The modelled solar cell exhibits a short-circuit current (J_{sc}) of 26.57 mA/cm^2, 0.7188 V open-circuit voltage (V_{oc}), fill factor (FF) of 70, and 13.37% efficiency (η). A value of 2.30 eV was recorded for the band gap. Also, electron affinity and Nyquist plot were obtained for the solar cells. Solar cells with thin absorber surface thickness will result in lower fabrication cost. This will open a new frontier for modelling of metal oxide based thin films solar cells especially Cu_2O thin films solar cells.

Graphical Abstract

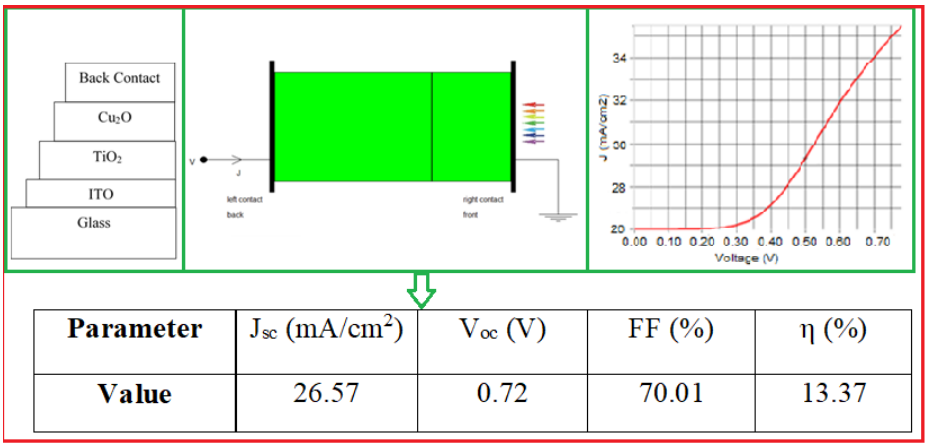

Parameter	J_{sc} (mA/cm^2)	V_{oc} (V)	FF (%)	η (%)
Value	26.57	0.72	70.01	13.37

Keywords: Cu_2O, Performance, Nanostructured, Thin films solar cells, surface thickness

* Corresponding author. Tel.: +27640827616 and +2348035431913; fax: +0-000-000-0000 .
E-mail address: ukobaking@yahoo.com

Nomenclature

Cu_2O:	Copper (I) oxide or cuprous oxide
CdTe:	Cadmium telluride
$CuInSe_2$:	The Copper Indium Selenium
Ti:	Titanium
O:	Oxygen
TiO_2:	Titanium oxide
ZnO:	Zinc oxide
CuO:	Copper oxide
In_2O_3:	Indium oxide
ITO:	Indium tin oxide
Au:	Gold
SPT:	Spray pyrolysis technique
J-V:	Current density-voltage
I-V:	Current-voltage
Voc:	Open-circuit voltage
Jsc:	Short-circuit current density
FF:	Fill factor
Pin:	Power in
Pmax:	Maximum power
SCAPS:	Solar Cell Capacitance Simulator

1. Introduction

The growing demand for energy and the adverse effect of fossil fuel on the planet continues to favor research on clean and sustainable energy. Nanostructured metal oxides continue to attract interest owing to their versatility in energy applications [1-4]. Nanostructured metal oxide (NMO) has good band gaps, affordable, tenable, abundant and environmentally friendly [5]. However, laboratory experimental results are yet to rival conventional silicon solar cells in terms of efficiency and performance. The numerical analysis of solar cells acts as a guidepost for faster and better experimental results [6]. Efficiency of solar cells is affected by several factors including the film surface thickness, surface roughness [7-8]. Hence, this study examined the effect of thickness and temperature with aim of improving the performance of Cu_2O/TiO_2 pn heterojunction solar cells.

Cuprous oxide (Cu_2O) solar cells have been studied lately. The cuprous oxide is low cost, plentiful, and non-hazardous, with over 20% under air mass 1 solar illumination [9]. It has an optical and direct band gap of 2.62 eV and 2.17eV respectively [10-11]. Cu_2O has a low affinity of 3.2eV [12]. It has high hole mobility of $256 cm^2V^{-1}s^{-1}$ and hole concentration of $1 \times 10^{14} cm^{-3}$ [13]. This makes Cu_2O a good hole transport p-type material in fabricating heterojunction solar cells. However, TiO_2 is an n-type material with a wide band gap in the range of 3.6eV to 3.2eV. TiO_2 has been studied greatly due to their favourable electronic and optical properties [14]. TiO_2 durability and high refractive index make the material useful for optical coating and anti-reflection coating. It is compatible with the n-type material used in heterojunction with several p-type materials [15].

Although, NMO still exhibits weak conversion efficiency with the maximum efficiency being around 8.4 % [16]. This has resulted in several duplications of resources in the laboratory in an attempt to achieve better efficiency comparable with those of CIGS solar cells of over 20 % [17]. Different laboratory procedures have been developed to deposit metal oxides with a view of obtaining better efficiency [18-21]. However, solar numerical analysis can be used to obtain improved efficiency without the bottleneck of experimental expenses. Solar numerical analysis has been around but mainly on solar panel and solar modules analysis. Although, few of such models were done using solar cells mainly of silicon and related solar cells [22-24].

Although, different tools can be used for simulation of thin film solar cells [25-29]. This study examined the effect of film thickness and temperature on the solar cells with aim of improving the performance [30]. This study model metal oxide heterojunction solar cells using Solar cells capacitance simulator (SCAPS). The metal oxide of Cu_2O and TiO_2 were modelled and a performance improvement has been observed. This is with a view of providing a useful guideline for the design of high performances metal oxide-based solar cells.

2. Methodology

2.1. The Mathematical Model

Solar cells are basically P-N heterojunction. Photovoltaic systems exhibit a nonlinear I –V characteristics that vary with the temperature of the solar cells and the radiant intensity. Under ideal condition, a solar cell can be theoretically modelled as a current source under a diode. A direct current is produced when the solar cells are exposed to light and this current varies linearly with the solar radiation. This is represented in Figure 1.

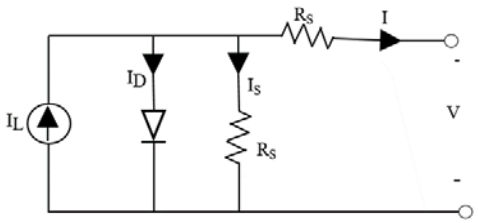

Fig 1. Solar cells model equivalent circuit

From the aforementioned, the characteristic equations are given as [31-32]:

$$I_{ph} = \frac{I_r \times I_{sc}}{I_{r0}} \quad (1)$$

Equation (1) shows that the photocurrent depends on the temperature of the solar cells and solar insolation.

$$V_t = \frac{kT}{q} \quad (2)$$

$$I_s = I_{sc} \times \left(e^{\left(\frac{V_{oc}}{n.V_t}\right)} - 1 \right) \quad (3)$$

It can be seen from equation (3) that the cell's saturation current varies with the cell temperature,

$$I_d = I_s \times \left(e^{\left(\frac{V + I.R_S}{n.V_t.N_S}\right)} - 1 \right) \quad (4)$$

Equation (4) gives the Shockley equation.

$$I = I_{ph} - I_d - I_{sh} \quad (5)$$

The output current of the solar cells is represented in Equation 5. Equations 1 to 5 give the electrical behaviour and relationship between the current supplied and voltage. Where; I_{ph} is photocurrent, I_{sc} is reverse saturation current, R_S and R_{sh} are inherent resistances in series and parallel associated with the cell, N_s is a number of cells in series, q is the electron charge, k is Boltzmann's constant and A is the ideality factor.

2.2. Background of the SCAPS analysis

SCAPS is a one-dimensional solar cells analysis program used for optoelectrical analysis of the 1-D or 2-D structures of semiconductor surfaces [33]. SCAPS is originally developed for cell structures of the $CuInSe_2$ and the CdTe family. However, there has been improvement in its capability, thereby making room for other types of solar cells. SCAPS uses finite difference methods to solve the differential equations along with several relations from the physics of semiconductors, and mathematically describe the performance of a solar cell. SCAPS performs a complete simultaneous numerical solution of the two continuity equations and Poisson's equation with the appropriate boundary conditions to one and two-dimensional cells [34]. The equations are expressed as shown in equations (6-8)

$$\nabla^2 v = -q/\in (p - n + N_D - N_A) \quad (6)$$

$$\nabla . J_p = q(G - R) \quad (7)$$

$$\nabla . J_n = q(R - G) \quad (8)$$

The general terms of 7 and 8 can be represented as:

$$G(x) = \int_0^{\infty} \phi a e^{-ax} d\lambda \quad (9)$$

The hole and electron current densities which appear in equations 7 and 8 are given by

$$J_p = -q\mu_p p \nabla V_p - kT\mu_p \nabla_p \quad (10)$$
$$J_n = -q\mu_n n \nabla V_n + kT\mu_n \nabla_n \quad (11)$$
$$V_p = V - (1-\gamma)\,\Delta G/g \quad (12)$$
$$V_n = V + \gamma\,\Delta G/g \quad (13)$$

Where v_p and v_n represent the effective potentials expressed in Equations 12 and 13. Δ_G and γ account for variations in the band structure, such as density of states and band gap, and account for Fermi-Dirac statistics. Expressions J_n and J_p represent the current density of the electron and holes respectively. Similarly, μ_n and μ_p represent the mobility of electron and hole respectively

2.3. SCAPS analysis of the Cu_2O/TiO_2 pn heterojunction

This study did performance improvement on Cu_2O/TiO_2 pn heterojunction using SCAPS (version 3.3.06). The input parameters of AM 1.5G lamp (power of 100 mW/m_2) at 300 K were used to compute the J-V photovoltaic properties of J_{SC}, V_{OC}, FF and η. The input parameters used for the SCAPs analysis were adapted from literature using properties and values of TiO_2 and Cu_2O and presented in Table 1 [13].

Table 1. Summary of input parameters used for the metal oxide SCAPS modelling [13]

Material properties	n-type TiO_2	p-type Cu_2O
Band Gap (eV)	2.26	2.17
Electron affinity	4.20	3.20
Dielectric permittivity (relative)	10.00	7.11
Conduction band ($1/cm^3$)	2.0E+17	2.0E+17
Valence band ($1/cm^3$)	6.0E+17	1.1E+19
Electron mobility (cm^2/Vs)	1.0E+2	2.0E+2
Hole mobility (cm^2/Vs)	25.0	8.0E+1
Shallow uniform donor density ($1/cm^3$)	1.0E+17	0
Shallow uniform acceptor density ($1/cm^3$)	0	1.0E+18

The input parameters for the back and front contact were optimized values using the SCAPS software and is shown in Table 2.

Table 2. Summary of input parameters for the back and front contact used for the metal oxide SCAPS analysis.

Parameter	Front contact	Back Contact
Holes	1.00E + 5	1.00E + 5
Electron	1.00E + 5	1.00E + 5
Metal Work function (eV)	5.0216	5
Majority Carrier Barrier height (eV) relative to E_f	0.2216	0.4
Majority Carrier Barrier height (eV) relative to E_v	0	0.2271

The solar cells schematic structure is shown in figure 2. The absorber surface known as the p-type is Cu_2O, the buffer surface known as n-type is TiO_2.

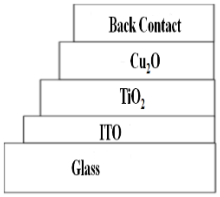

Fig 2. The Cu_2O/TiO_2 pn heterojunction structure

3. Results And Discussion

3.1. Effect of thickness

The film thickness was varied with aim of improving the performance of the solar cells. Previous study recommends absorber surface thickness of <1500 nm to obtain high efficiency [35]. Therefore, this study varied the absorber surface (Cu_2O) thickness between 100 nm to 600 nm, the buffer surface (TiO_2) between 50 nm to 100 nm and kept other properties constant. Figure 3 gives the SCAPS surface interface.

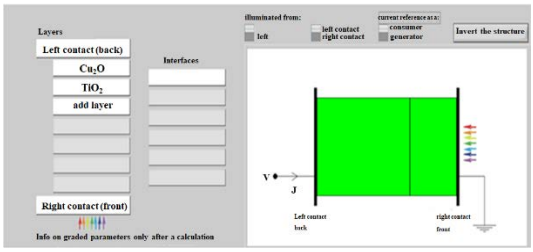

Fig 3. SCAPS panel showing the Cu_2O/TiO_2 Solar cells definition

Figure 4 depict the plot of the varied absorber surface thickness with the solar cells efficiency. The solar cells efficiency decreases with an increment in the absorber surface (TiO_2). An increase in the absorber surface (Cu_2O) results in more photons being absorbed culminating in photo generated current increment [36]. The optimized result gave a cell efficiency of 13.37 % at absorber surface thickness of 100 nm and buffer surface thickness of 50 nm which is an increment on existing result of 1.05% obtained via experimental electrochemical deposition of Cu_2O/TiO_2 heterojunction solar cells recorded by Saehana and Muslimin [37].

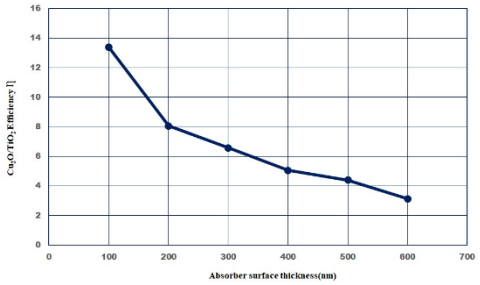

Fig 4. A plot of absorber surface thickness with the solar cells efficiency

Figure 5 shows the plot of the varied absorber and buffer surface thickness with the solar cells Fill Factor. The highest fill factor was obtained to be 70%. The FF decreased as the thickness increased. This agrees with the solar cells efficiency which also experienced a fluctuation at the same thickness.

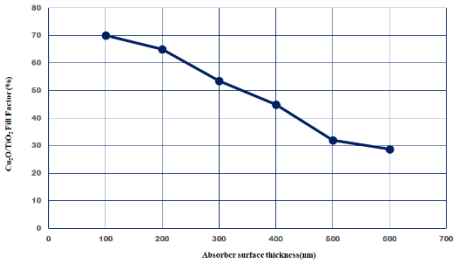

Fig 5. A plot of absorber and buffer surface thickness with the solar cells filled factor

3.2. Effect Of Temperature on the Solar Cell

Solar cells can be deposited using different techniques at different temperature [38]. This study was simulated using the SCAPS. The selected temperature range is between (0 to 400 ^{o}C) to accommodate room temperature, spin coating, spray pyrolysis, surface annealing. The effect of temperature on the open circuit voltage of the solar cells is shown in Figure 6. The open circuit voltage decreases with increment in deposition temperature. This decrease also results in decrease in efficiency. This may be ascribed to the fact that increase in hole and electron recombination result in reduction of hole and free electrons [39].

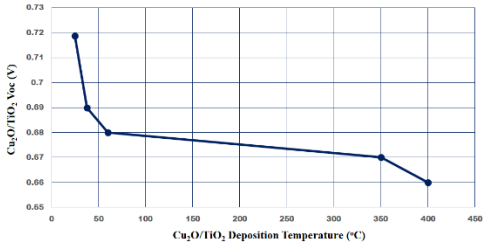

Fig 6. The effect of temperature on the open circuit voltage of Cu_2O/TiO_2 solar cells

3.3. Current-Voltage characteristic (J-V)

The J-V characteristic at room temperature in the dark shows that the forward current of the cells increases slowly with increasing voltage. The solar cell has rectification properties since the dark J-V plots were similar to the Shockley diode characteristics, which can be expressed by the standard diode equation [40].

$$J = J_0 \left[\exp\left(\frac{qv}{AkT}\right) - 1\right] \tag{14}$$

Where q is the electronic charge, A is the diode quality factor (ideality factor), k is Boltzmann's constant, T is the absolute temperature, and J_o is the reverse saturation current.

The simulated optimized J-V curve is shown in Figure 7. This is in concordance with the standard J-V curve of a solar cells under illumination [41].

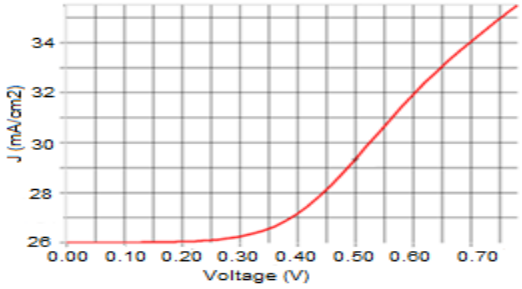

Fig 7. The J-V curve for the optimized Cu_2O/TiO_2 pn heterojunction

The efficiency is obtained using Equation 15 as shown below

$$\eta = \frac{FF \times (V_{OC} \times J_{SC})}{P_{in}} \quad (15)$$

The solar cell parameters evaluated from the J-V curve are presented in Table 3.

Table 3. The parameters of the Cu_2O/TiO_2 pn heterojunction solar cells.

Parameter	J_{sc} (mA/cm^2)	V_{oc} (V)	FF (%)	η (%)
Value	26.57	0.72	70.01	13.37

The modelled solar cell exhibits a short-circuit current (J_{sc}) of 26.57 mA/cm^2, the open-circuit voltage (V_{oc}) of 0.72 V, the fill factor (FF) of 70.01 %, and the efficiency (η) of 13.37%. This is a marked improvement in the efficiency of 1.05 obtained from the electrochemical deposition of Cu_2O/TiO_2 heterojunction solar cells recorded by Saehana, and Muslimin [37].

The grading energy parameter of the simulated solar cells is shown in Figure 8. It shows the band gap and electron affinity of the simulated solar cells. A value of 2.30 eV band gap was obtained which falls within the band gap range of Cu_2O.

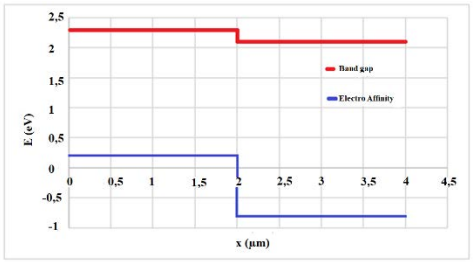

Fig 8. Grading Energy parameter of the Cu_2O/TiO_2 pn heterojunction solar cells.

3.4. Admittance Spectroscopy

It is a deep level characterization technique used to analyse deep levels in the depletion region of a metal-semiconductor junction or pn junction [42]. It measures the AC signal at different frequencies from a junction thereby enabling more information to be read from the trap. It is used to measure the Schottky-barrier admittance as a function of the temperature of the trapping levels [43]. It can also measure the conductance peaks as a function of temperature and frequency for capture coefficients and depth [44]. Equation 16 gives the depletion surface junction of the capacitance [45].

$$C_{Dep} = \frac{\varepsilon_r}{\omega} = \left(\frac{\varepsilon_r q N_A}{2V_{bi}}\right)^{1/2} \quad (16)$$

Where ω is the depletion surface width, q the elementary charge, ε_r the semiconductor's dielectric constant, N_A the acceptor concentration, and V_{bi} the built-in voltage.

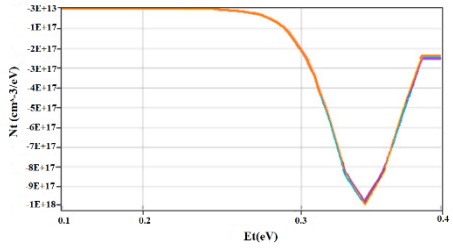

Fig. 9. A plot of N_t versus E_t for the Cu_2O/TiO_2 pn heterojunction solar cells

Figure 9 represents the curve of N_t against E_t for the solar cells. The three curves represent the p-type, n-type and the final solar device. The yellow is the final solar device with better result, the green is for Cu_2O and the red represent the TiO_2.

3.5. Effect of capacitance-voltage characteristic(C-V)

Figure 10 depicts the relationship between capacitance and voltage of the Cu_2O/TiO_2 pn heterojunction solar cells. The capacitance remained constant until applied voltage of 0.18volt and rose until 51.40 nF/cm^2. This increase in capacitance may be due to the excess minority carriers occupying the electronic density state. Also, the electronic state was observed to be dispersed in the band gap and movement of the Fermi level.

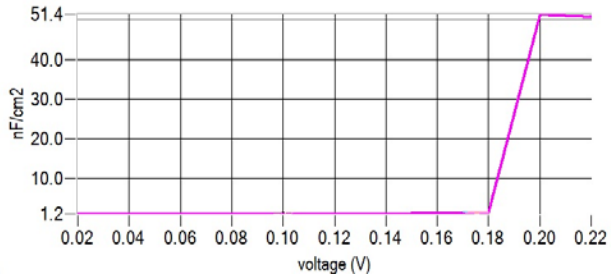

Fig. 10. A plot of capacitance versus applied voltage of Cu_2O/TiO_2 pn heterojunction solar cells

Figure 11 depicts the capacitance density against Gaussian energy distribution, E_t obtained from the admittance spectroscopy of the simulated Cu_2O/TiO_2 pn heterojunction solar cells. The three curves represent the p-type, n-type and the final solar device. The yellow is the final solar device with better result, the green is for Cu_2O and the red represent the TiO_2.

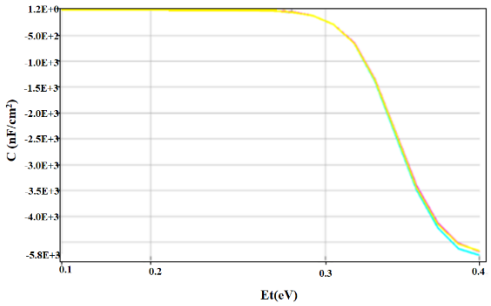

Fig. 11. A plot of capacitance density against Gaussian senergy distribution Et (eV) for the Cu_2O/TiO_2 pn heterojunction solar cells

Escape-frequency is a measure of the probability that an electron will occupy and break the bond. From Figure 11, the escape frequency of 1.00E+9 was obtained at 300k. The escape frequency of the commonly used commercial solar panel (a-Si) is giving to be $10^7 s^{-1}$ for a phonon frequency of 10^{13} semiconductor a-Si. Therefore, this study escape frequency is in agreement with earlier report value of 5×10^{-6} [46]. There is variation in the capacitance corresponding to the applied energy distribution. This variation indicates the arrangement of the electronic state in the bandgap and displacement of the Fermi level [47].

3.6. Effect of capacitance-frequency characteristic(C-F)

Figure 12 represents a plot of the capacitance of the simulated solar cells as a function of the corresponding frequency. A steady rise of the capacitance is recorded until it reaches a constant of 1.19 nF/cm^2 at a constant temperature of 300K. A typical capacitor decreases as the frequency across its plates increases [48], this means that the modelled heterojunction behaves like a capacitor until the value of 1.19 nF/cm^2 at the 300K. The capacitor is

charging or discharging as many electrons leave one terminal as arrive at the other. The three curves represent the p-type, n-type and the final solar device. The yellow is the final solar device with better result, the cyan is for Cu_2O and the red represent the TiO_2.

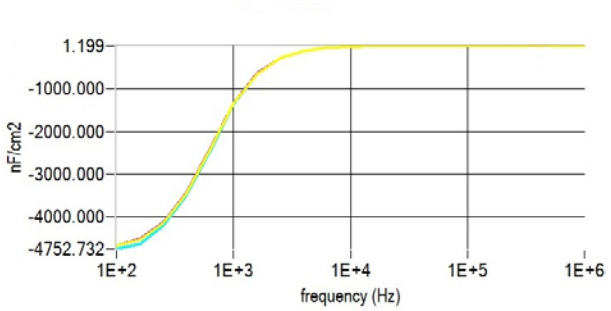

Fig. 12. Capacitance versus frequency of the Cu_2O/TiO_2 pn heterojunction solar cells

3.7. Effect of conductance-voltage characteristic(G-V)

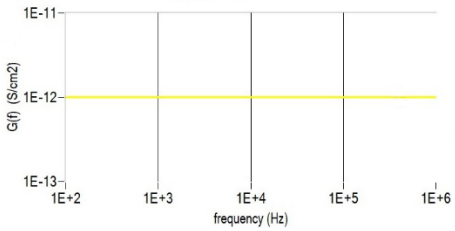

Fig. 13. A plot of conductance against frequency of Cu_2O/TiO_2 pn heterojunction solar cells

Figure 13 is a curve of the relationship between the conductance and frequency of the Cu_2O/TiO_2 pn heterojunction solar cells. There is change in the value of the conductance against the frequency. This show the ease with which electric current flows through the Cu_2O/TiO_2 pn heterojunction solar cells.

3.8. NYQUIST Plot

The Nyquist plot of Cu_2O/TiO_2 pn heterojunction solar cells is shown in Figure 14. This is the representation of the real and imaginary of the impedance (Z) of the simulated solar cells [49]. The three curves represent the p-type, n-type and the final solar device. The yellow is the final solar device with better result, the green is for Cu_2O and the cyan represent the TiO_2. The three curves represent the p-type, n-type and the final solar device. The yellow is the final solar device with better result, the purple is for Cu_2O and the cyan represent the TiO_2. It is used to determine the resistance (R_s and R_p) to obtain the equivalent electrical circuit of the solar cells [50]. A series resistance of 2.00 Ohms cm^2 was recorded for the Cu_2O/TiO_2 pn heterojunction solar cells. The greater the resistance the better the quality of the solar cells.

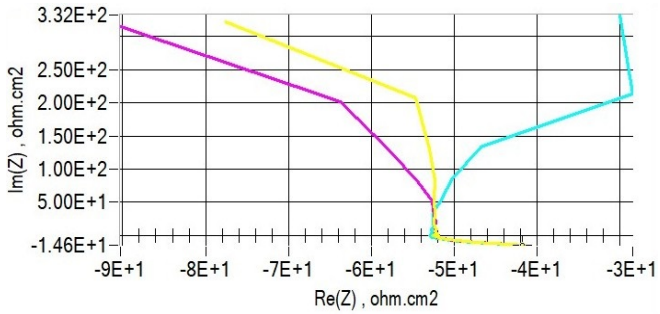

Fig. 14. Nyquist plot of the simulated Cu_2O/TiO_2 pn heterojunction solar cells

4. Conclusion

A metal oxide (Cu_2O/TiO_2) heterojunction solar cells was successfully modelled and performance improved performed using SCAPS. The performance improvement examined the effect of solar cells surface thickness, effect of deposition temperature and effect of other parameters on the solar cells properties especially the efficiency, fill factor, open circuit voltage and current density. An improved power conversion efficiency of 13.38%, short-circuit current (J_{sc}) of 0.2657 A, the open-circuit voltage (V_{oc}) of 0.7188 V, the fill factor (FF) of 0.70 was recorded. A value of 2.30 eV was recorded for the band gap. A thinner film thickness with improved efficiency means a reduction in the solar cells fabrication cost. This is positive indications of the potential of metal oxide as alternatives to other expensive and toxic solar cells materials. Experimental realization of this efficiency will require proper optimization of deposition variables and strict adherence.

Acknowledgements

The authors would like to acknowledge the SCAPS team for allowing us the use of the software. Also, authors would also like to acknowledge the financial support from NRF and URC of UJ.

References

[1] M. Diab, B. Moshofsky, I. Jen-La Plante, T. Mokari, A facile one-step approach for the synthesis and assembly of copper and copper-oxide nanocrystals. Journal of Materials Chemistry 21 (31) (2011) 11626-11630.

[2] M. Ge, C. Cao, J. Huang, S. Li, Z. Chen, K.Q. Zhang, S. S. Al-Deyab, Y. Lai, A review of one-dimensional TiO_2 nanostructured materials for environmental and energy applications. Journal of Materials Chemistry A, *4*(18), (2016) 6772-6801.

[3] R. Wick, S.D. Tilley, Photovoltaic and photoelectrochemical solar energy conversion with Cu_2O. The Journal of Physical Chemistry C, 119 (47) (2015) 26243-26257.

[4] T. Minami, Y. Nishi, T. Miyata, Heterojunction solar cell with 6% efficiency based on an n-type aluminum–gallium–oxide thin film and p-type sodium-doped Cu_2O sheet. Applied Physics Express. 8(2), (2015) 022301.

[5] W. M Djinkwi, S Ouédraogo, F. Tchoffo, F. Zougmoré, J.M.B. Ndjaka, Numerical investigations and analysis of Cu2ZnSnS4 based solar cells by SCAPS-1D. *International Journal of Photoenergy*, *2016*.

[6] C. C. Lee, P. C. Huang, J.Y. He, Layout designs of surface barrier coatings for boosting the capability of oxygen/vapor obstruction utilized in flexible electronics. Applied Surface Science. *436* (2018) 183-188.

[7] K. Wang, Z. Xu, F. Ling, Y. Wang, S. Dong, Annealing and thickness effects on magnetic properties of Co_2FeAl alloy films. *Applied Surface Science*. *435* (2018) 1125-1135.

[8] F. Feng, X. Zhang, T. Qu, B. Liu, J. Huang, J. Li, S. Xiao, Z Han, P. Feng, Surface scaling analysis of textured MgO thin films fabricated by energetic particle self-assisted deposition. *Applied Surface Science*, *437*, (2018) 287-293.

[9] L. Olsen, R. Bohara, M. Urie, Explanation for low-efficiency Cu_2O Schottky-barrier solar cells. Applied physics letters, 34(1) (1979) 47-49.

[10] B.K. Meyer, A. Polity, D, Reppin, M. Becker, P. Hering, P.J. Klar, T. Sander, C. Reindl, J. Benz, M. Eickhoff, C. Heiliger, Binary copper oxide semiconductors: From materials towards devices. *physica status solidi (b)*, *249*(8), (2012) 1487-1509.

[11] M. Heinemann, B. Eifert, C. Heiliger, Band structure and phase stability of the copper oxides Cu_2O, CuO, and Cu_4O_3. Physical Review B, 87(11) (2013) 115111.

[12] M.I. Hossain, F.H. Alharbi, N. Tabet, Copper oxide as inorganic hole transport material for lead halide perovskite based solar cells. Solar Energy, 120 (2015) 370-380.

[13] B. Li, K. Akimoto, A. Shen, Growth of Cu_2O thin films with high hole mobility by introducing a low-temperature buffer layer. Journal of Crystal Growth, 311(4) (2009) 1102-1105.

[14] R. Rivera, A. Stashans. Defects in TiO_2 crystals. in Proceedings of the International MultiConference of Engineers and Computer Scientists. 2013.

[15] C. Frisk, T. Ericson, S.Y. Li, P. Szaniawski, J. Olsson, C. Platzer-Björkman, Combining strong interface recombination with bandgap narrowing and short diffusion length in Cu2ZnSnS4 device modeling. *Solar Energy Materials and Solar Cells*, *144*, (2016) 364-370.

[16] B. Shin, O. Gunawan, Y. Zhu, N.A. Bojarczuk, S.J. Chey, S. Guha, Thin film solar cell with 8.4% power

conversion efficiency using an earth-abundant Cu_2ZnSnS_4 absorber. *Progress in Photovoltaics: Research and Applications*, *21*(1), (2013) 72-76.
[17] H. Liu, V. Avrutin, N. Izyumskaya, U. Özgür, H. Morkoç, Transparent conducting oxides for electrode applications in light emitting and absorbing devices. *Superlattices and Microstructures*, *48*(5), (2010) 458-484.
[18] K. Ukoba, A. Eloka-Eboka, F. Inambao, Review of nanostructured NiO thin film deposition using the spray pyrolysis technique. Renewable and Sustainable Energy Reviews, 82 (2018) 2900-2915.
[19] P.C. McIntyre, Y. Oshima, E. Kim, K.C. Saraswat, Interface studies of ALD-grown metal oxide insulators on Ge and III–V semiconductors. *Microelectronic Engineering*, *86*(7-9), (2009) 1536-1539.
[20] D.M. Mattox, Handbook of physical vapor deposition (PVD) processing. 2010: William Andrew.
[21] H. Kim, Atomic layer deposition of metal and nitride thin films: Current research efforts and applications for semiconductor device processing. Journal of Vacuum Science & Technology B: Microelectronics and Nanometer Structures Processing, Measurement, and Phenomena, 21(6) (2003) 2231-2261.
[22] P.P. Altermatt, Models for numerical device simulations of crystalline silicon solar cells—a review. Journal of computational electronics, 10(3) (2011) 314.
[23] J.G. Fossum, Computer-aided numerical analysis of silicon solar cells. Solid-State Electronics, 19(4) (1976) 269-277.
[24] A. Ingenito, M. Zeman, O. Isabella, Opto-electrical surface engineering of wafer based c-Si solar cells. 2016.
[25] S. Banerjee, Performance analysis of cadmium sulfide/cadmium telluride (CdS/CdTe) thin film solar cell using PC1D. in Devices for Integrated Circuit (DevIC), 2017. 2017. IEEE.
[26] T. Salmi, M. Bouzguenda, A. Gastli, A. Masmoudi, Matlab/simulink based modeling of photovoltaic cell. International Journal of Renewable Energy Research, *2*(2), (2012) 213-218.
[27] P. Ghosh, P.K. Kundu, Modeling and Simulation of Solar Cell using Embedded MATLAB Simulink Tool. International Journal of Electronics, Electrical and Computational System, 6(7) (2017) 101-114.
[28] N. Hernandez-Como, A. Morales-Acevedo, Simulation of hetero-junction silicon solar cells with AMPS-1D. Solar Energy Materials and Solar Cells, 94(1) (2010) 62-67.
[29] Y. Liu, Y. Sun, A. Rockett, A new simulation software of solar cells—wxAMPS. Solar Energy Materials and Solar Cells, 98 (2012) 124-128.
[30] M. Wang, D. Wang, P. Schaaf, Layer thickness effect on fracture behavior of Al/Si_3N_4 multilayer on Si substrate under three-point bending. *Applied Surface Science*, *445*, (2018) 563-567.
[31] GC Enebe, K Ukoba T.C Jen, Numerical modeling of effect of annealing on nanostructured CuO/TiO2 pn heterojunction solar cells using SCAPS. AIMS Energy, 7(4) (2019) 527–538.
[32] B. Alsayid, Modeling and simulation of photovoltaic cell/module/array with two-diode model. *International Journal of Computer Technology and Electronics Engineering*, 1(3), (2012) 6-11.
[33] M. Burgelman, K. Decock, S. Khelifi, A. Abass, Advanced electrical simulation of thin film solar cells. *Thin Solid Films*, *535*, (2013) 296-301.
[34] R. Schwartz, J. Gray, M. Lundstrom, Current status of one-and two-dimensional numerical models: Successes and limitations. 1985.
[35] N. Khoshsirat, N. A.M. Yunus, M.N Hamidon, S. Shafie, N. Amin, Analysis of absorber and buffer layer band gap grading on CIGS thin film solar cell performance using SCAPS. Pertanika Journal of Science and Technology, 23(2), (2015) 241-250.
[36] T. Zhai, X. Fang, M Liao, X. Xu, H Zeng, B. Yoshio, D. Golberg, A comprehensive review of one-dimensional metal-oxide nanostructure photodetectors. *Sensors*, *9*(8), (2009) 6504-6529.
[37] S. Saehana, Muslim, Performance Improvement of Cu_2O/TiO_2 Heterojunction Solar Cell by Employing Polymer Electrolytes. International Journal of Engineering & Technology, 13(6) (2013) 83-86.
[38] M.A. Green, Thin-film solar cells: review of materials, technologies and commercial status. *Journal of Materials Science: Materials in Electronics* 18, no. 1 (2007) 15-19.
[39] F. Anwar, S. Afrin, S. S. Satter, R. Mahbub, S.M. Ullah, Simulation and performance study of nanowire CdS/CdTe solar cell. *Int. J. Renewable Energy Research*, *7*(2), (2017) 885-893.
[40] K.O. Ukoba, F.L. Inambao, A.C. Eloka-Eboka, Fabrication of affordable and sustainable solar cells using NiO/TiO2 PN heterojunction. International Journal of Photoenergy, 2018(2018).
[41] E. Shi, L. Zhang, Z. Li, P. Li, Y. Shang, Y. Jia, J. Wei, K. Wang, H. Zhu, D. Wu, S. Zhang, TiO2-coated carbon nanotube-silicon solar cells with efficiency of 15%. *Scientific reports*, *2*, (2012) 884.
[42] E.F. Schubert, Doping in III-V semiconductors. 2015: E. Fred Schubert.
[43] D. Losee, Admittance spectroscopy of impurity levels in Schottky barriers. Journal of Applied Physics, 46(5)

(1975) 2204-2214.
[44] D. Losee, Admittance spectroscopy of deep impurity levels: ZnTe Schottky barriers. Applied Physics Letters, 21(2) (1972) 54-56.
[45] A.S. Kavasoglu, H. Bayhan, Admittance and Impedance Spectroscopy on Cu(In,Ga)Se_2 Solar Cells. Turkish Journal of Physics, 27(6) (2004) 529-536.
[46] Kuo, Y. ed., 2001. Thin Film Transistor Technologies V: Proceedings of the International Symposium. The Electrochemical Society.
[47] D. Diallo, A.K. Ehemba, A. Ndiaye, M.M. Soce, M. Dieng, The influence of the thickness of the Cds emitter layer on the performance of a CIGS solar cell with acceptor defects. *International Journal of Engineering and Applied Sciences*, *4*(1) (2017) 1-4.
[48] M. Innocent, P. Wambacq, S. Donnay, H.A. Tilmans, W. Sansen, H. De Man, An analytic Volterra-series-based model for a MEMS variable capacitor. IEEE Transactions on Computer-Aided Design of Integrated Circuits and Systems, 22(2), (2003) 124-131.
[49] K. Pandey, P. Yadav, I. Mukhopadhyay, Elucidating different mass flow direction induced polyaniline–ionic liquid interface properties: insight gained from DC voltammetry and impedance spectroscopy. The Journal of Physical Chemistry B. 118(11) (2014) 3235-3242.
[50] S. Kumar, P. K. Singh, G. S. Chilana, S. R. Dhariwal, Generation and recombination lifetime measurement in silicon wafers using impedance spectroscopy. *Semiconductor Science and Technology* 24, no. 9 (2009) 095001.